De Novo *KCNB1* Mutations in Epileptic Encephalopathy

Ali Torkamani, PhD,[1] Kevin Bersell, MA,[2] Benjamin S. Jorge, BA,[3] Robert L. Bjork, Jr, MD,[4,5] Jennifer R. Friedman, MD,[6] Cinnamon S. Bloss, PhD,[1] Julie Cohen, MS,[7] Siddharth Gupta, MD,[7,8] Sakkubai Naidu, MD,[7,8] Carlos G. Vanoye, PhD,[9,10] Alfred L. George, Jr, MD,[2,9,10] and Jennifer A. Kearney, PhD[9,10]

Objective: Numerous studies have demonstrated increased load of de novo copy number variants or single nucleotide variants in individuals with neurodevelopmental disorders, including epileptic encephalopathies, intellectual disability, and autism.
Methods: We searched for de novo mutations in a family quartet with a sporadic case of epileptic encephalopathy with no known etiology to determine the underlying cause using high-coverage whole exome sequencing (WES) and lower-coverage whole genome sequencing. Mutations in additional patients were identified by WES. The effect of mutations on protein function was assessed in a heterologous expression system.
Results: We identified a de novo missense mutation in *KCNB1* that encodes the $K_V2.1$ voltage-gated potassium channel. Functional studies demonstrated a deleterious effect of the mutation on $K_V2.1$ function leading to a loss of ion selectivity and gain of a depolarizing inward cation conductance. Subsequently, we identified 2 additional patients with epileptic encephalopathy and de novo *KCNB1* missense mutations that cause a similar pattern of $K_V2.1$ dysfunction.
Interpretation: Our genetic and functional evidence demonstrate that *KCNB1* mutation can result in early onset epileptic encephalopathy. This expands the locus heterogeneity associated with epileptic encephalopathies and suggests that clinical WES may be useful for diagnosis of epileptic encephalopathies of unknown etiology.

ANN NEUROL 2014;76:529–540

Epileptic encephalopathies are a heterogeneous group of severe childhood onset epilepsies characterized by refractory seizures, neurodevelopmental impairment, and poor prognosis.[1] The developmental trajectory is normal prior to seizure onset, after which cognitive and motor delays become apparent. Ongoing epileptiform activity adversely affects development and contributes to functional decline. Therefore, early diagnosis and intervention may improve long-term outcomes.[2–4]

Recently, there has been significant progress in identifying genes responsible for epileptic encephalopathies, and de novo mutations have been reported in approximately a dozen genes, including *SCN1A*, *SCN2A*, *SCN8A*, *KCNQ2*, *HCN1, GABRA1*, *GABRB3*, *STXBP1*, *CDKL5*, *CHD2*, *SYNGAP1*, and *ALG13*.[5–9] The majority of mutations reported are in genes encoding voltage-gated ion channels, neurotransmitter receptors, and synaptic proteins. There is significant phenotype

View this article online at wileyonlinelibrary.com. DOI: 10.1002/ana.24263

Received Jun 2, 2014, and in revised form Aug 25, 2014. Accepted for publication Aug 26, 2014.

Address correspondence to Dr Kearney, Department of Pharmacology, Northwestern University, Searle 8-510, 320 East Superior St, Chicago, IL 60611. E-mail: jennifer.kearney@northwestern.edu

From the [1]Scripps Translational Science Institute, Scripps Health, and Scripps Research Institute, San Diego, CA; [2]Department of Pharmacology and [3]Vanderbilt Brain Institute, Vanderbilt University, Nashville, TN; [4]Department of Pediatrics, Scripps Health, San Diego, CA; [5]Sea Breeze Pediatrics, San Diego, CA; [6]Departments of Neurosciences and Pediatrics, University of California, San Diego, San Diego, CA; [7]Kennedy Krieger Institute, Baltimore, MD; [8]Department of Pediatrics, Johns Hopkins University School of Medicine, Baltimore, MD; [9]Department of Medicine, Vanderbilt University, Nashville, TN; and [10]Department of Pharmacology, Northwestern University Feinberg School of Medicine, Chicago, IL.

Additional supporting information can be found in the online version of this article.

heterogeneity, with mutations in the same gene resulting in different clinical presentations, as well as locus heterogeneity, with mutations in different genes resulting in the same syndrome. Furthermore, epileptic encephalopathy genes have substantial overlap with genes responsible for other neurodevelopmental disorders, including autism and intellectual disability.[10–12]

Due to the considerable phenotype and locus heterogeneity, it is difficult to predict appropriate candidate genes for testing in a particular patient. Therefore, hypothesis-free approaches such as whole exome sequencing (WES) or whole genome sequencing (WGS) may be useful for uncovering causative variations in epileptic encephalopathies of unknown etiology. Thus, we aimed to identify the underlying genetic cause of epileptic encephalopathy in the proband by WES and WGS of a family quartet.

Subjects and Methods

Study Subjects

Study participants included ID9, parents ID9F and ID9M, and an unaffected sister ID9S. Adults provided written informed consent, with additional assent by ID9 and ID9S, under a protocol approved by the Scripps institutional review board. Consent for release of medical information for individual 2 was obtained from the parents. Clinical details are described below and summarized in Table 1.

Individual ID9 is a 9-year-old female with epileptic encephalopathy, hypotonia, developmental delays, cognitive impairment, and intermittent agitation. Pre- and perinatal histories were unremarkable, although hypotonia and excessive somnolence were noted early. Motor milestones were delayed, with sitting at 9 months, walking at 20 months, and persistent clumsiness. Language acquisition was delayed, with regression at age 18 months. Motor, language, and behavior have fluctuated, but overall there has been forward developmental progress. Onset of generalized tonic–clonic seizures (GTCS) was at 4.75 years of age, although behavioral manifestations likely representing other seizure types were present earlier. Multiple seizure semiologies were reported, including rare GTCS, head drops, and more common facial twitching with drooling, eye fluttering, gagging, vomiting, and stiffening. Rare GTCS are controlled with levetiracetam and clonazepam, but other seizure types have been poorly controlled with multiple therapies that were ineffective or limited by side effects (see Table 1). In addition, the patient experiences sumatriptan-responsive migrainous episodes consisting of headache, abdominal discomfort, photophobia, and lethargy.

Brain magnetic resonance imaging (MRI) showed subtle asymmetric volume loss in left hippocampus. Recent 7-day video electroencephalographic (EEG) monitoring revealed mild diffuse slowing and abundant bihemispheric multifocal epileptiform discharges more prominent in right temporal and midparietal regions. Electroclinical seizures began in the left hemisphere, with 2 in centroparietal areas and 1 without clear localization. Magnetoencephalography showed frequent epileptiform spikes during sleep (648 spikes observed over 50 minutes), with frequent trains of spikes. Source modeling showed epileptiform spike activity arising from bilateral posterior perisylvian regions. The first cluster of spikes (~55%) originated from the anterior–inferior aspect of the left parietal lobe, extending to the left superior temporal gyrus. The second cluster of spikes (~45%) originated from the right temporal–parietal junction. No propagations were observed.

Muscle biopsy showed type 1 fiber predominance with mild generalized hypertrophy. There was slight elevation of plasma guanidinoacetate at 2.5μM (normal range: 0.3–2.1μM) but not in the range typically associated with disease. There was mild elevation of cerebrospinal fluid (CSF) pyruvate (147μM, normal range: 0–75μM) with normal lactate (2.06mM, normal range: 0.5–2.2mM). CSF 5-methyltetrahydrofolate was mildly reduced at 36nM (normal range: 40–128nM). Folinic acid therapy has had unclear impact. Extensive additional workup was normal and included: karyotype, fragile X and Angelman syndrome testing, comparative genome hybridization oligo-single nucleotide polymorphism array, mitochondrial DNA Southern blot and mitochondrial DNA sequencing, plasma acylcarnitine, creatine phosphokinase, uric acid, biotinidase, ammonia, vitamin B12, folate, homocysteine, folate receptor antibodies, lymphocyte pyruvate dehydrogenase activity, urine organic acids, urine creatine and guanidinoacetate, CSF glucose, protein, amino acids, neurotransmitter metabolite levels and pterins, muscle carnitine, coenzyme Q10, and electron transport chain complex analysis.

Individual 2 presented as a 2-year-, 10-month-old male with poor seizure control, developmental delay, absent speech, stereotyped handwringing movements, and progressive inturning of feet requiring orthotic support. Prenatal and perinatal histories were normal. Development plateaued at 6 months and seizures began at 8 months of age, with hypsarrythmic EEG, for which he was treated with adrenocorticotropic hormone. Although seizures were resistant to conventional treatment, a gluten/casein/sugar/starch-free diet begun at 2.5 years of age resulted in seizure reduction to 3/day despite marked spike activity demonstrable on EEG. At 4 years of age, seizures worsened and L-carnitine was added with subsequent amelioration. At 5 years of age, EEG was persistently abnormal, with epileptiform discharges of multifocal origin including bursts of diffuse polyspikes, diffuse polyspike-wave, right temporal spike and wave, left occipital spikes, and diffuse polyspike bursts lasting up to 4 minutes. Brain MRI studies at 9 months did not show structural, neuronal migration, or white matter abnormalities. He began walking at 2.5 years, and is presently interactive socially, although nonverbal. Extensive additional workup was normal. Genetic testing for mutations associated with *SCN1A*, *MECP2*, *CDKL5*, *FOXG1*, *ARX*, and fragile X, Pitt–Hopkins, and Angelman syndromes were negative. Tests for plasma and CSF amino acid concentrations, urine organic acid levels, CSF neurotransmitter levels, lysosomal enzymes, very long chain fatty acids, neuronal ceroid lipofuscinosis 1 and 2, urine

TABLE 1. Clinical Features in 3 Individuals with Epileptic Encephalopathy and *KCNB1* Missense Mutations

Individual	Current Age, yr/Sex	Age at Onset	Seizure Types	Seizure Control with Antiepileptic Therapies? (treatments)	Developmental Delay	Brain MRI	EEG	Other	Family History of Epilepsy	Presumed Causal Variant	Amino Acid Change	Predicted Consequence: Provean [score], SIFT [score], Polyphen2 [score]
ID9	9/F	4 years	Tonic–clonic; tonic; atonic; focal; focal with secondary generalization	No (topiramate, clobazam, levetiracetam, Depakote, carbamazepine, lacosamide, clonazepam, oxcarbazepine)	Yes, motor and language	Subtle volume loss in left hippocampus	Mild diffuse slowing and abundant bihemispheric multifocal epileptiform discharges	Hypotonia, strabismus, migraine;	No	Chr20: 47991056, G/T	S347R	Deleterious [−4.996], damaging [0.003], probably damaging [0.995]
2	7/M	8 months	Tonic–clonic; atonic; focal; infantile spasms	No (ACTH, topiramate, Depakote, pyridoxine, ketogenic diet)	Yes, motor and language	Normal	Hypsarrhythmia; diffuse polyspikes, diffuse polyspike-wave, right temporal spike and wave, left occipital spikes, and series of bursts of diffuse polyspikes	Hypotonia, strabismus, tremulousness, nonverbal, stereotyped handwringing movements, in-turning of feet	No	Chr20: 47990962, C/T	G379R	Deleterious [−7.926], damaging [0.000], probably damaging [1.000]
3, Coriell ND27062	5/F	0 years	Tonic–clonic; atonic; focal dyscognitive atypical absence; infantile spasms	Unknown	Yes, unspecified	Normal	Unspecified	Cerebral palsy	Yes, absence epilepsy in great uncle	Chr20: 47990976, G/A	T374I	Deleterious [−5.945], damaging [0.000], probably damaging [0.999]

ACTH = adrenocorticotropic hormone; EEG = electroencephalogram; F = female; M = male; MRI = magnetic resonance imaging.

TABLE 2. Whole Exome and Whole Genome Sequencing Coverage

Sample	Whole Exome Sequencing		Whole Genome Sequencing	
	Coverage, Mean	Target Exome with at Least 10 Reads, %	Coverage, Mean	Genome Redundancy of 5 Reads, %
ID9, proband	109	94.5	4.1	37.9
ID9F, father	109	94.6	6.0	66.7
ID9M, mother	124	94.9	6.9	75.2
ID9M, sister	97	94.2	7.2	77.4

sulfocysteine, congenital disorders of glycosylation, and oligoarray were all normal. Clinical WES was performed by GeneDx, and reported variants were confirmed by Sanger sequencing.

Individual 3 (Coriell ND27062) was ascertained by the Epilepsy Phenome/Genome Project[13] as part of a patient cohort with infantile spasms and/or Lennox–Gastaut syndrome.[5] Seizure onset occurred during the first year of life, and seizure types have included tonic–clonic, atypical absence, atonic, infantile spasms, and focal dyscognitive (see Table 1). EEG findings were unspecified; imaging studies were reported as normal.

Whole Exome, Whole Genome Sequencing, Variant Calling, and Filtration

Genomic DNA was extracted from blood using the QiaAmp system (QIAGEN, Valencia, CA). Enriched exome libraries were prepared using the SureSelect XT enrichment system (Agilent, Santa Clara, CA). WES was performed on an Illumina (San Diego, CA) HiSeq2500 instrument with indexed, 100 base pair (bp), paired-end sequencing. Reads were mapped to the hg19 reference genome using Burrows–Wheeler transform[14]; variant calling and quality filtration were performed using Genome Analysis Toolkit best practices variant quality score recalibration.[15–17] Mean coverage of 97- to 124-fold was achieved for each subject with 94 to 95% of the target exome covered by >10 reads (Table 2). Libraries for low-pass WGS were prepared using the NEBNext DNA Library Prep System (New England Biolabs, Ipswich, MA). WGS was performed on an Illumina HiSeq2500 with 100-bp indexed, paired-end sequencing. Mean coverage of 4- to 7-fold was achieved for each subject with ~64.3% of the genome covered by >5 reads (see Table 2). Copy number variants (CNVs) were identified by CNVNator.[18]

Variant annotation was performed using SG-ADVISER (Scripps Genome Annotation and Distributed Variant Interpretation Server; http://genomics.scripps.edu/ADVISER/) as previously described.[19] A series of filters were applied to derive a set of candidate disease-causing variants (Table 3): (1) population-based filtration removed variants present at >1% allele frequency in the HapMap,[20] 1000 Genomes,[21] National Heart, Lung, and Blood Institute Exome Sequencing Project (http://evs.gs.washington.edu/EVS/), or Scripps Wellderly populations (individuals older than 80 years with no common chronic conditions sequenced on the Complete Genomics platform); (2) annotation-based filtration removed variants in segmental duplication regions that are prone to produce false-positive variant calls due to mapping errors[22]; (3) functional impact-based filtration retained only variants that are nonsynonymous, frameshift, nonsense, or affect canonical splice-site donor/acceptor sites, and (4) inheritance-based filters removed variants not present in the trio in a manner consistent with affectedness status. Following filtering, retained variants were confirmed by Sanger sequencing.

Locus-Specific Mutation Rate Estimate

The *KCNB1* locus-specific mutation rate was determined as described.[23] Human and chimpanzee alignments of the protein coding portion of exons and intronic essential splice sites were considered. The *KCNB1* mutation rate per site is 2.71×10^{-3} differences per bp of aligned sequence. Assuming a divergence time of 12 million years between chimpanzee and human and a

TABLE 3. Whole Exome Sequencing Variant Filtration for Individual ID9

Variant Type	No. in Family
Total variants	101,797
Rare variants, <1% allele frequency	18,475
Not in segmental duplication	13,463
Nonsynonymous, truncating, or splice site	1,053
De novo inheritance	2
Homozygous or compound heterozygous inheritance	3

25-year average generation time, the *KCNB1* locus-specific mutation rate per site per generation is 5.65×10^{-9}. The probability of observing de novo mutation events was estimated using the Poisson distribution:

$$P(X;\mu) = [(e^{-\mu})(\mu^X)]/X!$$

where X is the number of de novo events observed and μ is the average number of de novo events based on the locus-specific mutation rate.

Plasmids and Cell Transfection

Mutations were introduced into full-length human $K_V2.1$ cDNA engineered in plasmid pIRES2-Ds-Red-MST[24] by QuikChange mutagenesis (Agilent). Wild-type human $K_V2.1$ cDNA was subcloned into the pIRES2-smGFP expression vector. Expression of wild-type and mutant $K_V2.1$ in CHO-K1 cells was achieved by transient transfection using FUGENE-6 (Roche, Basel, Switzerland) and 0.5μg of total cDNA (1:1 mass ratio). Expression of wild-type alone was achieved by transfection with pIRES2-smGFP-WT-$K_V2.1$ plus empty pIRES2-DsRed-MST, whereas expression of mutant alone was performed with pIRES2-DsRed-MST-mutant-$K_V2.1$ and empty pIRES2-smGFP. Coexpression of mutant and wild-type was achieved by cotransfection with pIRES2-smGFP-WT-$K_V2.1$ and pIRES2-DsRed-MST-mutant-$K_V2.1$ or pIRES2-dsRed-MST-WT-$K_V2.1$. Following transfection, cells were incubated for 48 hours before use in experiments.

Cell Surface Biotinylation

Proteins on the surface of CHO-K1 cells transfected with wild-type and/or mutant $K_V2.1$ were labeled with cell membrane-impermeable Sulfo-NHS-Biotin (Thermo Scientific, Waltham, MA). Following quenching with 100mM glycine, cells were lysed and centrifuged. Supernatant was collected and an aliquot was retained as the total protein fraction. Biotinylated surface proteins (100μg per sample) were recovered from the remaining supernatant by incubation with streptavidin-agarose beads (Thermo Scientific) and eluted in Laemmli sample buffer. Total (1μg per lane) and surface fractions were analyzed by Western blotting using mouse anti-$K_V2.1$ (1:500; NeuroMab, Davis, CA; clone K89/34), mouse anti-transferrin receptor (1:500; Invitrogen, Carlsbad, CA; #13-6800), rabbit anti-calnexin (H70; 1:250; Santa Cruz Biotechnology, Santa Cruz, CA; sc-11397) primary antibodies, and peroxidase-conjugated mouse anti-rabbit immunoglobulin G (IgG; 1:100,000; Jackson ImmunoResearch, West Grove, PA) and goat anti-mouse IgG (1:50,000, Jackson ImmunoResearch) secondary antibodies. Blots were probed for each protein in succession, stripping in between with Restore Western Blot Stripping Buffer (Pierce Biotechnology, Rockford, IL). Western blot analysis was performed in triplicate on samples from 3 independent transfections. The order of anti-$K_V2.1$ and anti-transferrin receptor antibodies was alternated, with transferrin receptor probed first in 2 of 3 experiments. Selectivity of biotin labeling for cell surface was confirmed by probing with calnexin following detection of $K_V2.1$ and transferrin receptor. Calnexin signal was consistently present in total protein lanes and absent in surface fraction lanes. Densitometry was performed using NIH ImageJ software. To control for protein loading, $K_V2.1$ bands were normalized to the corresponding transferrin receptor band. For each genotype, the normalized values were then expressed as a ratio of surface to total expression. Normalized total, surface, and surface:total ratios were compared between genotypes using 1-way analysis of variance.

Electrophysiology

Whole cell patch clamp recordings were performed as previously described,[24] except that recording solutions were altered to achieve appropriate voltage control. The external solution contained (in millimolars): 132 *X*Cl (where *X* is Na^+ except when molar substitution has been made for K^+, Rb^+, or N-methyl-D-glucamine $[NMDG]^+$), 4.8 KCl, 1.2 $MgCl_2$, 2 $CaCl_2$, 10 glucose, and 10 HEPES, pH 7.4. The internal solution contained (in millimolars): 20 K-aspartate, 90 NMDG-Cl, 1 $MgCl_2$, 1 $CaCl_2$, 11 ethyleneglycoltetraacetic acid (EGTA), 10 HEPES, and 5 K_2ATP, pH 7.3. When cells expressing mutant channels alone or coexpressed with wild-type Kv2.1 (Kv2.1-WT) were held at −80mV, they exhibited large currents that prevented adequate voltage control. Therefore, a holding potential of −30mV was used for experiments. Whole cell currents were measured from −80 to +60 mV (in 10mV, 500-millisecond-long steps) from a holding potential of −30mV followed by a 500-millisecond step to 0mV (tail currents). Voltage dependence of activation was evaluated from tail currents measured 10 milliseconds after stepping to 0mV from −40mV to +30mV and fit to the Boltzmann equation. Kinetic analysis of activation rate was performed by exponential fit of the first 50 milliseconds of current induced after a voltage step from the holding potential.

For cation selectivity experiments, recording solutions were altered as follows. Sucrose dilution was performed by adding 300mM sucrose solution 10:1 (vol/vol) to the external solution described above. For determining permeability ratios, the internal solution was modified to contain (in millimolars): 110 K-aspartate, 1 $MgCl_2$, 1 $CaCl_2$, 11 EGTA, 10 HEPES, and 5 K_2ATP, pH 7.3, and equimolar replacement of extracellular sodium with the monovalent cations K^+, Rb^+, and $NMDG^+$. The permeability ratio (P_X/P_{Na}) was calculated from measured reversal potentials (E_{rev}) according to the following equation[25]:

$$E_{\text{rev}} = (\mathbf{R}T/\mathbf{F}) \ln(P_x[X^+]_o/P_{Na}{}^+[\text{Na}^+]_i$$

where **R** is the gas constant, T is absolute temperature, **F** is Faraday's constant, X^+ is the monovalent cation in the extracellular solution, and P_X is permeability of the X^+ cation.

Data for each experimental condition were collected from ≥3 transient transfections, and analyzed and plotted using Clampfit (Molecular Devices, Sunnyvale, CA) and Prism 5 (GraphPad Software, La Jolla, CA). Currents were normalized for membrane capacitance and shown as mean ± standard error of the mean, and number of cells used for each experimental condition is listed in Table 4. Statistical significance was

TABLE 4. Voltage Dependence of Activation for WT and Mutant $K_V2.1$ Channels

Channel	Mean $V_{1/2}$ ± SEM	Slope factor ± SEM	No.
Kv2.1-WT	−4.1 ± 1.5	4.4 ± 0.4	12
Kv2.1-WT + G379R	1.3 ± 2.0[a]	5.2 ± 0.6	8
Kv2.1-WT + S347R	2.8 ± 1.6[a]	5.9 ± 0.5	8
Kv2.1-WT + T374I	1.9 ± 1.5[a]	5.7 ± 0.2	7

[a]$p < 0.05$.
SEM = standard error of the mean; WT = wild type; $V_{1/2}$ = voltage for half-maximal channel activation.

determined using unpaired Student *t* test (GraphPad). Probability values are provided in the figures or figure legends.

Results

We employed WES (∼100× coverage) and WGS (∼5× coverage) of the proband (ID9), unaffected father (ID9F), unaffected mother (ID9M), and unaffected sister (ID9S) to identify the molecular cause of an epileptic encephalopathy. Filtering of WES variants was done under the assumption that disease in ID9 was the result of a heterozygous de novo mutation, but we also considered simple and compound recessive models. Variants discovered by WES were processed through a series of filters based on population, variant annotation, functional impact, and inheritance to identify a set of candidate disease-causing variants (see Table 3). Sequence coverage and detailed variant data are presented in Table 2 and the Supplementary Table. CNVs were also interrogated by WGS; however, no CNVs consistent with disease segregation were identified. This process identified de novo missense variants in 2 candidate genes, *KCNB1* and *MLST8* (Table 5). Under other genetic models, we identified a homozygous missense variant in *HRNBP3* and compound heterozygous variants in *NLRP1* and *BAHCC1*. Of all the identified variants, the *KCNB1* variant was deemed the most likely candidate based on the de novo inheritance pattern, the function of *KCNB1* and its relationship to other epilepsy genes, and the predicted deleterious consequence on protein function by multiple algorithms. *KCNB1* encodes the alpha subunit of the $K_V2.1$ voltage-gated potassium channel, a delayed rectifier

TABLE 5. Inheritance of Validated Candidate Variants in Individual ID9

Gene	ID1 Status	Amino Acid Change	WES Genotype				Predicted Consequence		
			ID9	ID9F	ID9M	ID9S	Provean	SIFT	Polyphen2
KCNB1	De novo	S347R	01	00	00	00	Deleterious (−4.996)	Damaging (0.003)	Probably damaging (0.995)
MLST8	De novo	Q302R	01	00	00	00	Neutral (−2.12)	Tolerated (0.203)	Benign (0.114)
HRNBP3	Homozygous	Y5H	11	01	01	00	Deleterious (−3.54)	Damaging (0.000)	Benign (0.446)
NLRP1	Compound heterozygous	V939M	01	00	01	01	Neutral (−2.08)	Damaging (0.006)	Probably damaging (0.982)
		R834C	10	01	00	00	Neutral (−0.46)	Tolerated (0.216)	Benign (0.000)
BAHCC1	Compound heterozygous	A941T	01	00	01	01	Neutral (−1.38)	Tolerated (0.215)	Benign (0.009)
		E1990K	10	01	00	00	Neutral (−0.91)	Tolerated (0.168)	Possibly damaging (0.900)

Genotypes: 0 = reference allele; 1 = alternate allele.
WES = whole exome sequencing.

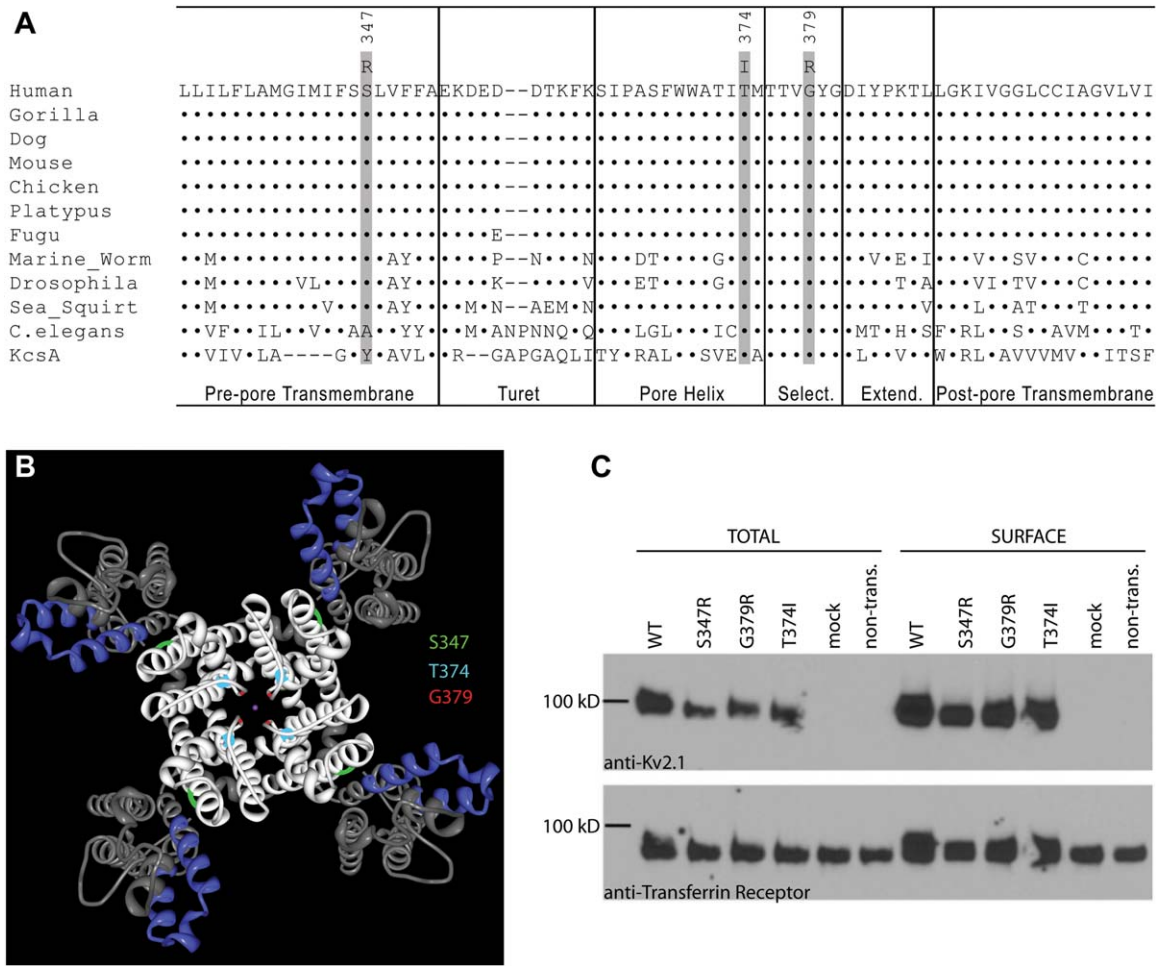

FIGURE 1: K_V2.1 mutations identified in 3 individuals with epileptic encephalopathy. (A) Evolutionary conservation of K_V2.1. Multiple alignment of K_V2.1 species orthologs (Clustal Omega[38]) is shown. Mutated amino acids are shaded, and functional subdomains of the pore region are indicated. (B) Location of mutations mapped onto the crystal structure of a K_V2.1/K_V1.2 chimera (PDB 29R9).[39] A channel tetramer is shown from the extracellular side. S347 (green) lies at the interface between the voltage sensor (blue) and pore (white) domains. T374 (teal) lies adjacent to the selectivity filter, whereas G379 (red) lies in the selectivity filter. (C) Mutant K_V2.1 proteins are expressed and trafficked to the cell surface. Cell surface expression was measured using cell surface biotinylation of CHO-K1 cells transfected with wild-type (WT) or mutant K_V2.1. Total and surface fractions of K_V2.1 were detected with anti-K_V2.1 antibody. Endogenous transferrin receptor levels were measured as a loading control. The blot was probed first with anti-transferrin receptor, stripped, and then reprobed with anti-K_V2.1.

potassium channel that is an important regulator of neuronal excitability. The S347R variant is located in the pore domain that is necessary for ion selectivity and gating (Fig 1).

We identified 2 additional unrelated patients with epileptic encephalopathy and de novo missense variants in *KCNB1* discovered by WES. Individual 2 presented with a sporadic epileptic encephalopathy of unknown cause (see Table 1). After a series of negative genetic and metabolic tests, he was referred for clinical WES. From that analysis it was determined that he had a single de novo missense variant in *KCNB1*. The variant G379R, located in the selectivity filter of K_V2.1, was predicted to be deleterious by functional impact algorithms (see Fig 1, Table 1). Additional inherited variants included a heterozygous splice site mutation in the *NPC2* gene (IVS4+1 G>A) inherited from his unaffected father and a variant of unknown significance in *GRIN2A* (A1276G) inherited from his unaffected mother. Neither of these transmitted variants was thought to be causative for the principal phenotypes of individual 2, although they may contribute by modifying overall expression of the clinical phenotype. Inheritance of Nieman Pick disease type 2C (NPC2) is generally recessive, and the clinical phenotype of individual 2 was not consistent with NPC type 2. The *GRIN2A* A1276G variant is a known single nucleotide variant that was inherited from the unaffected mother and exists in the general population (0.1% minor allele frequency in European Americans). A1276G is a

conservative substitution in an alternatively spliced portion of the *GRIN2A* gene at a position that does not show a high degree of evolutionary conservation and was predicted to be benign by multiple functional impact algorithms (Provean: neutral [−0.78]; SIFT: tolerated [0.284]; Polyphen2: benign [0.376]).

Individual 3 was recently reported as part of an epileptic encephalopathy exome sequencing study by the Epi4K consortium.[5] She presented with early onset epileptic encephalopathy and cerebral palsy (see Table 1). A de novo missense variant in *KCNB1* was reported for individual 3, with no additional de novo variants reported.[5] The variant T374I is located in the pore domain of $K_V2.1$ and was predicted to be deleterious by functional impact algorithms (see Fig 1, Table 1).

Given the locus-specific mutation rate of *KCNB1* (5.65×10^{-9} mutation rate/base/generation), the probability of identifying 3 independent mutations is low ($p < 1.1 \times 10^{-13}$), providing statistical evidence that these variants may be pathogenic. The altered residues show a very high degree of evolutionary conservation (see Fig 1A), with T374 and G379 being invariant through the ancestral KcsA bacterial potassium channel. Furthermore, all 3 *KCNB1* variants are located in the functionally important pore domain of the $K_V2.1$ channel protein. Serine 347 is located in the prepore transmembrane segment, and threonine 374 is located in the pore helix. Glycine 379 is part of the critical GYG motif that defines the potassium selectivity filter (see Fig 1A, B).

Effects of the *KCNB1* variants on $K_V2.1$ channel function were evaluated following transient expression in CHO-K1 cells. Expression of each mutant in CHO-K1 cells resulted in total and cell surface expression similar to the wild-type channel, with no significant genotype-dependent differences in total ($F_{3,8} = 1.767$, $p = 0.213$), surface ($F_{3,8} = 0.017$, $p = 0.997$), and surface:total ($F_{3,8} = 0.266$, $p = 0.848$) expression of Kv2.1. This indicates that the mutations do not interfere with protein expression or trafficking to the cell surface (see Fig 1C). Expression of $K_V2.1$-WT resulted in large voltage-dependent potassium currents with characteristic outward rectification and late inactivation (Fig 2B, C). In contrast, expression of each of the 3 mutants yielded small currents with linear current–voltage relationships. These aberrant currents were blocked by gadolinium (Gd^{3+}), strongly suggesting that the currents are pore-mediated (Fig 3). Based upon the external and internal K^+ concentrations used in these experiments, the theoretical reversal potential (E_{rev}) for K^+-selective currents is −47mV. Expression of the mutant channels produced currents with depolarized E_{rev} (S347R: -23.2 ± 4.8mV; G379R: $-14{\cdot}0 \pm 4.5$mV; T374I: $-16{\cdot}5 \pm 5.5$mV), indicating that the mutations affect ion selectivity. To test ion selectivity, the external solution was diluted 1:10 with 300mM sucrose. Under these conditions, a depolarizing shift in E_{rev} would indicate anion selectivity, whereas a hyperpolarizing shift would indicate cation selectivity. Dilution of the extracellular solution produced a hyperpolarizing shift in E_{rev}, confirming the current conducted was cation-selective (Fig 4). Changes in cation selectivity were determined by measuring changes in E_{rev} following molar replacement of extracellular sodium with monovalent cations. All 3 mutants exhibited loss of K^+ selectivity, with K^+/Na^+ permeability ratios of 0.9 compared to the reported 14:1 ratio for Kv2.1-WT.[26]

To investigate the effects of the mutant channels in a heterozygous background, we coexpressed each mutant with Kv2.1-WT channel and compared to the wild-type channel expressed alone. Coexpression of $K_V2.1$-WT with T374I, S347R, or G379R resulted in reduced current measured at test potentials ranging from 0 to +60mV (see Fig 2C), depolarizing shifts in the voltage-dependence of steady-state activation (see Figs 2D and 5, Table 4), and greater time constants of activation (τ) measured from +30 to +60mV test potentials (see Figs 2E and 5). The observed changes in kinetic parameters suggest that the mutant and wild-type subunits can form heterotetrameric channels.

Discussion

Co-occurrence of de novo variants in *KCNB1* in 3 independent patients with overlapping clinical phenotypes that include epileptic encephalopathy with associated cognitive and motor dysfunction provides strong genetic evidence that the *KCNB1* variants are likely pathogenic. Further evidence for a pathogenic effect of the *KCNB1* mutations comes from functional studies of mutant $K_V2.1$ channels. All 3 mutations, located within the pore domain of $K_V2.1$, resulted in channels with similar dysfunctional features.

Previous studies demonstrated that mutations in the pore region can result in altered ion selectivity.[27–30] Consistent with this, each $K_V2.1$ mutant exhibited voltage-independent, nonselective cation currents. When coexpressed with wild-type channels, all Kv2.1 mutants induced depolarizing shifts in the voltage dependence of activation and reduced current density at more depolarized voltages. Furthermore, coexpression of the Kv2.1 mutants with wild-type channels resulted in inward currents in the voltage range where $K_V2.1$ channels are normally closed, as evidenced by large inward currents

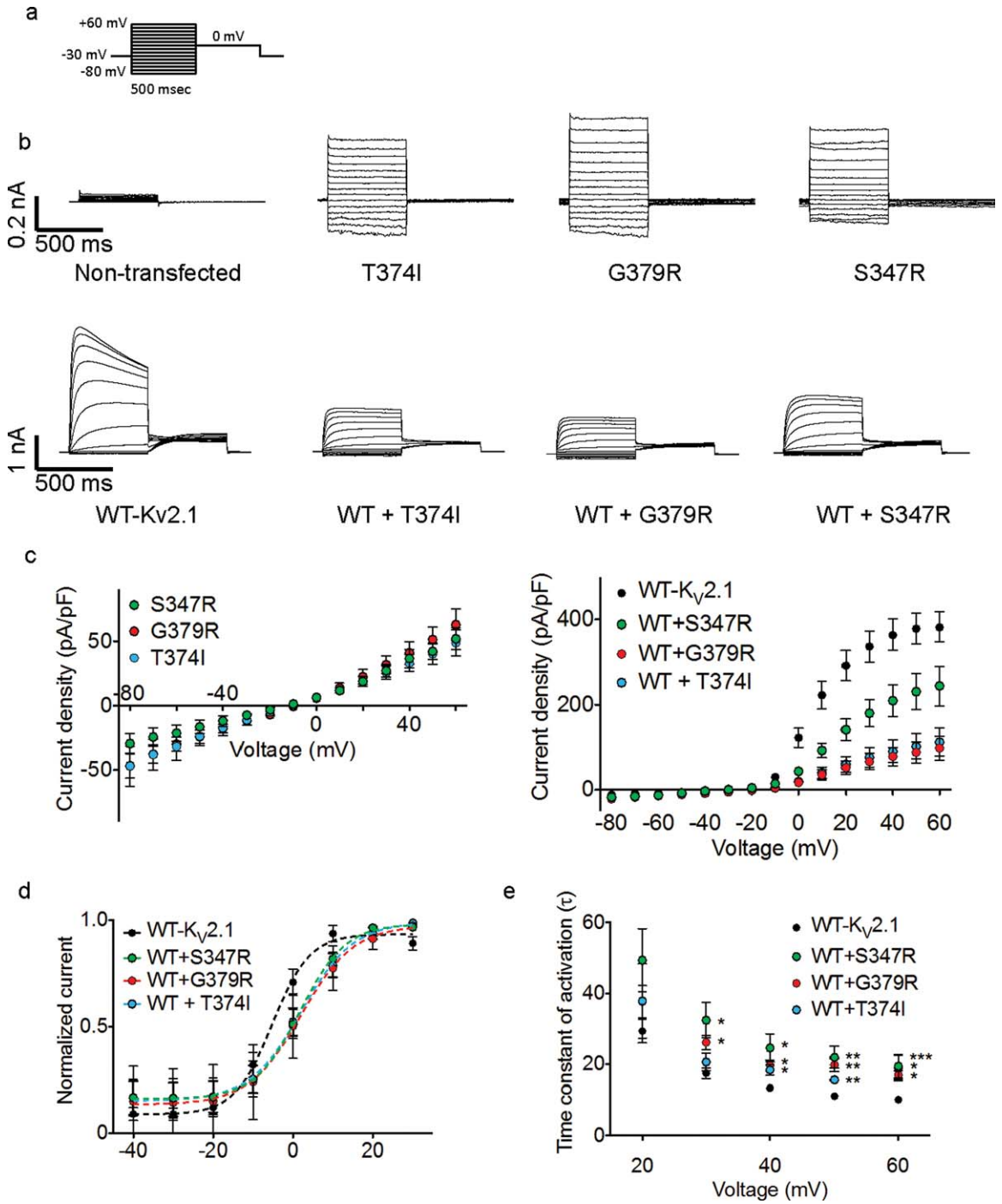

FIGURE 2: Functional consequence of K_V2.1 mutations. (A) CHO-K1 cells were held at −30mV, and whole cell currents were recorded from −80 to +60mV in 10mV steps for 500 milliseconds followed by a 500-millisecond step to 0mV to record tail currents. (B) Average whole cell current traces recorded from nontransfected CHO-K1 cells and CHO-K1 cells transiently expressing wild-type (WT) or mutant (G379R, S347R, T374I) K_V2.1 channels, or coexpressing WT plus mutant channels. (C) Current density–voltage relationships measured from CHO-K1 cells expressing mutant or WT, or coexpressing WT and mutant K_V2.1 channels. Currents were normalized to cell capacitance (picofarads). WT plus mutant channels had significantly decreased current density at test potentials ranging from 0 to +60mV compared to WT alone ($P<0.05$). (D) Voltage dependence of steady-state activation. Tail currents were normalized to peak amplitude and fit with Boltzmann function. Biophysical parameters of voltage dependence are detailed in Table 4. (E) The time constant of activation was determined from exponential fit of individual current traces. *$P<0.05$, **$P<0.005$, ***$P<0.0001$.

observed when using a holding potential of −80mV. These gain-of-function and dominant-negative functional defects are predicted to result in depolarized resting membrane potential and impaired membrane repolarization, with increased cellular excitability as a net consequence.

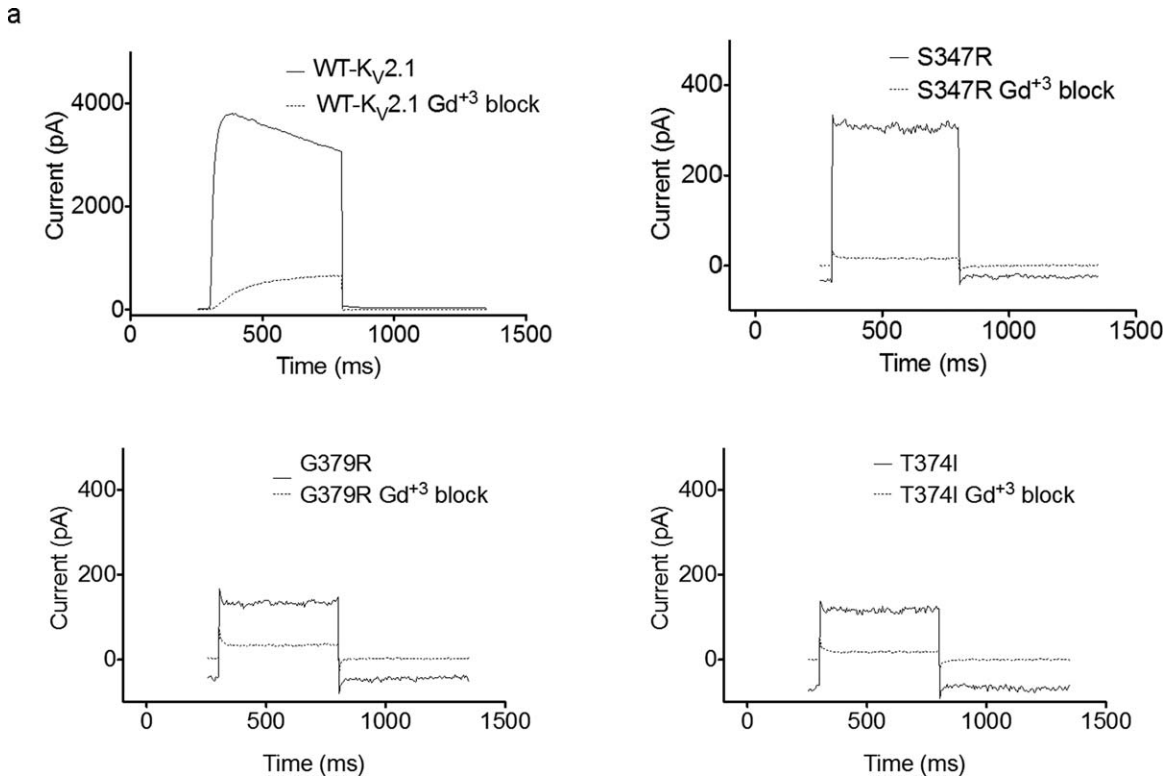

FIGURE 3: $GdCl_3$ block of mutant K_V2.1 channels. Representative traces are shown of control and Gd^{3+} block at +60 mV of wild-type (WT; 86 ± 2.1%, n = 5) or mutant channels (S347R; 94 ± 3.7%, n = 3), G379R (79 ± 4.2%, n = 4), and T374I (94 ± 2.5%, n = 3).

K_V2.1 is the main contributor to delayed rectifier potassium current in pyramidal neurons of the hippocampus and cortex.[31–35] Delayed rectifier potassium current is critical for membrane repolarization under conditions of repetitive stimulation and acts to dampen high-frequency firing. Reduction of delayed rectifier potassium current by *Kcnb1* deletion in mice results in reduced thresholds to induced seizures, but not spontaneous seizures.[36] This suggests that loss of K_V2.1 function predisposes neuronal networks to hyperactivity, resulting in a modest increase in seizure risk. In contrast, our results demonstrate that gain-of-function and dominant-negative effects result in epileptic encephalopathy. A similar phenomenon is observed with *KCNQ2* wherein heterozygous loss-of-function mutations result in benign familial neonatal seizures, whereas mutations with dominant-negative effects result in epileptic encephalopathy.[37] This suggests that variable functional defects resulting from different mutations in the same gene contribute to the pleiotropic effects observed for genes associated with neurodevelopmental disorders.

In summary, our genetic and functional evidence identifies mutation of *KCNB1* as a cause of epileptic encephalopathy. This expands the considerable locus heterogeneity associated with epileptic encephalopathies,[5,6]

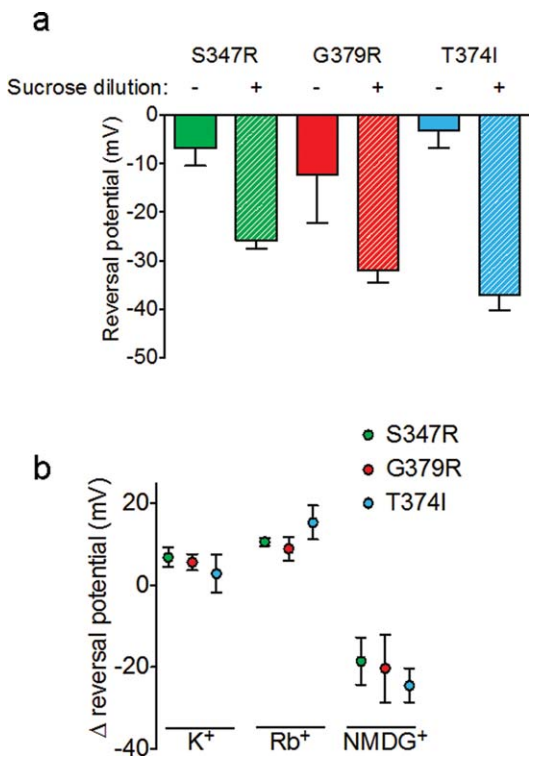

FIGURE 4: Ion selectivity of mutant K_V2.1 channels. (A) Reversal potentials were determined by linear fit to $y = mx + b$, where m is the slope and b is the y-intercept, in control bath and after bath was diluted 10-fold in 300mM sucrose solution. (B) Change in reversal potential after equimolar substitution of extracellular monovalent Na^+. NMDG = N-methyl-D-glucamine.

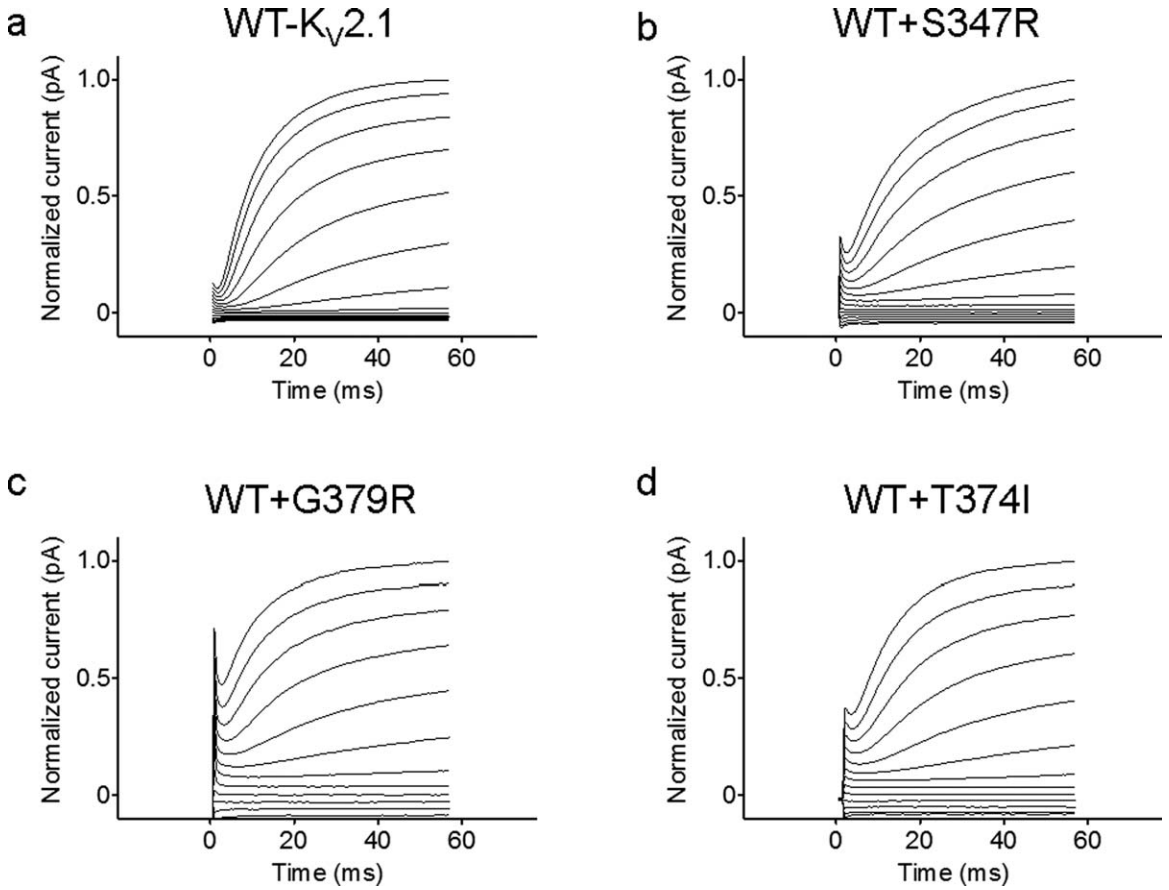

FIGURE 5: Expanded view of whole cell current traces for evaluation of activation kinetics of wild-type (WT) K_V2.1 channel alone or coexpressed with mutant channels. Expanded view is shown of the first 50 milliseconds of whole cell currents following voltage change from −80mV to +60mV and normalized to peak current recorded from CHO-K1 cells transiently expressing (A) K_V2.1-WT or coexpressing WT and mutant K_V2.1 channels (B) S347R, (C) G379R, and (D) T374I.

suggesting that clinical exome sequencing may be useful for molecular diagnosis. Rapid genetic diagnosis is beneficial for appropriate disease management and may improve long-term outcomes in epileptic encephalopathies.[2–4]

Acknowledgment

This work was supported by Scripps Genomic Medicine, an NIH National Center for Advancing Translational Sciences Clinical and Translational Science Award (5 UL1 RR025774) to Scripps Translational Science Institute, as well as funding from the Shaffer Family Foundation and the Anne and Henry Zarrow Foundation. Further support is from NIH/NHGRI U01 HG006476 (A.T.), NIH/NINDS R01 NS053792 (J.A.K.), NIH/NINDS R01 NS032387 (A.L.G.), and NIH/NINDS F31 NS083097 (B.S.J.).

We thank the patients and their families for their cooperation; S. E. Topol, G. Zhang, and J. Lee for technical contributions; and the members of our IDIOM (Idiopathic Disease of Man) review panel for their dedication and support: Drs K. Bethel, J. Diamant, S. Haaser, N. Hywnn, E. Kavalerchik, B. Patay, J. Sheard, R. Simon, and G. Williams.

Authorship

Experiments were conceived by A.T., C.S.B., J.A.K., and A.L.G. Patient phenotyping and review were performed by R.L.B., J.R.F., J.C., S.G., and S.N. Sequence data analysis and statistical interpretation were performed by A.T. and J.A.K. Functional evaluation of mutations was performed and analyzed by K.B., B.S.J., C.G.V., A.L.G., and J.A.K. The manuscript was written by A.T., A.L.G., and J.A.K., and reviewed by all authors. A.T., K.B., and B.S.J. contributed equally.

Potential Conflicts of Interest

A.T.: founder, stockholder, consultant, Cypher Genomics; patent pending, 118537-003PCT (licensee: Cypher Genomics). J.R.F.: husband is a biotech investor with investments in the sequence analysis and therapeutics space. A.L.G.: grant, Gilead Sciences.

References

1. Berg AT, Berkovic SF, Brodie MJ, et al. Revised terminology and concepts for organization of seizures and epilepsies: report of the ILAE Commission on Classification and Terminology, 2005–2009. Epilepsia 2010;51:676–685.
2. Berg AT, Loddenkemper T, Baca CB. Diagnostic delays in children with early onset epilepsy: impact, reasons, and opportunities to improve care. Epilepsia 2014;55:123–132.
3. Brunklaus A, Dorris L, Ellis R, et al. The clinical utility of an SCN1A genetic diagnosis in infantile-onset epilepsy. Dev Med Child Neurol 2013;55:154–161.
4. Hirose S, Scheffer IE, Marini C, et al. SCN1A testing for epilepsy: application in clinical practice. Epilepsia 2013;54:946–952.
5. Allen AS, Berkovic SF, Cossette P, et al. De novo mutations in epileptic encephalopathies. Nature 2013;501:217–221.
6. Carvill GL, Heavin SB, Yendle SC, et al. Targeted resequencing in epileptic encephalopathies identifies de novo mutations in CHD2 and SYNGAP1. Nat Genet 2013;457:825–830.
7. O'Brien JE, Meisler MH. Sodium channel SCN8A (Nav1.6): properties and de novo mutations in epileptic encephalopathy and intellectual disability. Front Genet 2013;4:213.
8. Nava C, Dalle C, Rastetter A, et al. De novo mutations in HCN1 cause early infantile epileptic encephalopathy. Nat Genet 2014; 46:640–645.
9. Veeramah KR, Johnstone L, Karafet TM, et al. Exome sequencing reveals new causal mutations in children with epileptic encephalopathies. Epilepsia 2013;54:1270–1281.
10. O'Roak BJ, Vives L, Girirajan S, et al. Sporadic autism exomes reveal a highly interconnected protein network of de novo mutations. Nature 2012;485:246–250.
11. Rauch A, Wieczorek D, Graf E, et al. Range of genetic mutations associated with severe non-syndromic sporadic intellectual disability: an exome sequencing study. Lancet 2012;380:1674–1682.
12. Sanders SJ, Murtha MT, Gupta AR, et al. De novo mutations revealed by whole-exome sequencing are strongly associated with autism. Nature 2012;485:237–241.
13. Abou-Khalil B, Alldredge B, Bautista J, et al. The epilepsy phenome/genome project. Clin Trials 2013;10:568–586.
14. Li H, Durbin R. Fast and accurate short read alignment with Burrows-Wheeler transform. Bioinformatics 2009;25:1754–1760.
15. McKenna A, Hanna M, Banks E, et al. The Genome Analysis Toolkit: a MapReduce framework for analyzing next-generation DNA sequencing data. Genome Res 2010;20:1297–1303.
16. DePristo MA, Banks E, Poplin R, et al. A framework for variation discovery and genotyping using next-generation DNA sequencing data. Nat Genet 2011;43:491–498.
17. Van der Auwera GA, Carneiro M, Hartl C, et al. From FastQ data to high-confidence variant calls: the Genome Analysis Toolkit best practices pipeline. Curr Protoc Bioinformatics 2013;43:11.10.1–11.10.33.
18. Abyzov A, Urban AE, Snyder M, Gerstein M. CNVnator: an approach to discover, genotype, and characterize typical and atypical CNVs from family and population genome sequencing. Genome Res 2011;21:974–984.
19. Chen YZ, Friedman JR, Chen DH, et al. Gain-of-function ADCY5 mutations in familial dyskinesia with facial myokymia. Ann Neurol 2014;75:542–549.
20. Altshuler DM, Gibbs RA, Peltonen L, et al. Integrating common and rare genetic variation in diverse human populations. Nature 2010;467:52–58.
21. Abecasis GR, Auton A, Brooks LD, et al. An integrated map of genetic variation from 1,092 human genomes. Nature 2012;491: 56–65.
22. Bailey JA, Gu Z, Clark RA, et al. Recent segmental duplications in the human genome. Science 2002;297:1003–1007.
23. O'Roak BJ, Vives L, Fu W, et al. Multiplex targeted sequencing identifies recurrently mutated genes in autism spectrum disorders. Science 2012;338:1619–1622.
24. Jorge BS, Campbell CM, Miller AR, et al. Voltage-gated potassium channel KCNV2 (Kv8.2) contributes to epilepsy susceptibility. Proc Natl Acad Sci U S A 2011;108:5443–5448.
25. Hille B. Ion channels of excitable membranes. Sunderland, MA: Sinauer Associates, 2001.
26. Consiglio JF, Andalib P, Korn SJ. Influence of pore residues on permeation properties in the Kv2.1 potassium channel. Evidence for a selective functional interaction of K+ with the outer vestibule. J Gen Physiol 2003;121:111–124.
27. Choi M, Scholl UI, Yue P, et al. K+ channel mutations in adrenal aldosterone-producing adenomas and hereditary hypertension. Science 2011;331:768–772.
28. Dibb KM, Rose T, Makary SY, et al. Molecular basis of ion selectivity, block, and rectification of the inward rectifier Kir3.1/Kir3.4 K(+) channel. J Biol Chem 2003;278:49537–49548.
29. Heginbotham L, Lu Z, Abramson T, MacKinnon R. Mutations in the K+ channel signature sequence. Biophys J 1994;66:1061–1067.
30. Navarro B, Kennedy ME, Velimirovic B, et al. Nonselective and G betagamma-insensitive weaver K+ channels. Science 1996;272: 1950–1953.
31. Du J, Haak LL, Phillips-Tansey E, et al. Frequency-dependent regulation of rat hippocampal somato-dendritic excitability by the K+ channel subunit Kv2.1. J Physiol 2000;522(pt 1):19–31.
32. Guan D, Tkatch T, Surmeier DJ, et al. Kv2 subunits underlie slowly inactivating potassium current in rat neocortical pyramidal neurons. J Physiol 2007;581:941–960.
33. Guan D, Horton LR, Armstrong WE, Foehring RC. Postnatal development of A-type and Kv1- and Kv2-mediated potassium channel currents in neocortical pyramidal neurons. J Neurophysiol 2011; 105:2976–2988.
34. Guan D, Armstrong WE, Foehring RC. Kv2 channels regulate firing rate in pyramidal neurons from rat sensorimotor cortex. J Physiol 2013;591:4807–4825.
35. Liu PW, Bean BP. Kv2 channel regulation of action potential repolarization and firing patterns in superior cervical ganglion neurons and hippocampal CA1 pyramidal neurons. J Neurosci 2014;34: 4991–5002.
36. Speca DJ, Ogata G, Mandikian D, et al. Deletion of the Kv2.1 delayed rectifier potassium channel leads to neuronal and behavioral hyperexcitability. Genes Brain Behav 2014;13:394–408.
37. Orhan G, Bock M, Schepers D, et al. Dominant-negative effects of KCNQ2 mutations are associated with epileptic encephalopathy. Ann Neurol 2014;75:382–394.
38. Sievers F, Wilm A, Dineen D, et al. Fast, scalable generation of high-quality protein multiple sequence alignments using Clustal Omega. Mol Syst Biol 2011;7:539.
39. Long SB, Tao X, Campbell EB, MacKinnon R. Atomic structure of a voltage-dependent K+ channel in a lipid membrane-like environment. Nature 2007;450:376–382.